



Effect of polygon order on additively manufactured lattice structures: a method for defining the threshold resolution for lattice geometry

A. Alghamdi¹ · B. Lozanovski^{1,2} · M. McMillan¹ · R. Tino^{1,2} · D. Downing^{1,2} · X. Zhang¹ · I. Kelbassa³ · P. Choong^{2,4} · M. Qian^{1,2} · M. Brandt^{1,2} · M. Leary^{1,2}

Received: 13 January 2019 / Accepted: 17 July 2019 / Published online: 31 October 2019
© Springer-Verlag London Ltd., part of Springer Nature 2019

Abstract

Additive manufacture (AM) enables the fabrication of highly efficient lattice structures. However, the mathematical efficiency of characterising AM lattice geometry can be poor, potentially restricting the commercial application of AM lattice structures. This research quantifies the effect of the polygon order used to characterise the geometric resolution of lattice strut elements on the associated manufacturability and geometric qualities of the manufactured lattice. The effect of these design parameters on manufactured quality is experimentally determined for aluminium and titanium specimens fabricated by selective laser melting (SLM), although the method can be generally applied to any AM technology. This research finds that geometric thresholds exist, below which additional geometric resolution does not result in increased part quality. These thresholds are a function of material, lattice inclination angle, cross-sectional area and the polynomial order used to represent the cross section. These findings enable significantly reduced computational cost in managing AM lattice structures, and can be directly integrated with algorithmic methods for the optimisation of AM lattice structures.

Keywords Selective laser melting (SLM) · Electron beam melting (EBM) · Lattice · Design for additive manufacture · Stereolithographic (STL) file format

1 Introduction

Additive manufacture (AM) enables the design of innovative and low-cost components that are infeasible by traditional manufacturing methods [35]. In particular, metal additive manufacture (MAM) enables the fabrication of complex lattice structures with unique engineering properties that provide commercial advantage [8], in numerous industry sectors including:

- High-value aerospace applications with robust engineering properties. For example, Sexton et al. [27] demonstrated laser cladding of aerospace components, including turbine blades with Rene and Inconel nickel-based superalloys. Brandt et al. [4] present a procedure for topology optimisation integrated with MAM technical requirements such that high-value aerospace components are designed in a systematic manner.
- Patient-specific implant manufacture. For example, Vandenbroucke and Kruth [31] initially characterised the mechanical properties and biocompatibility for Ti6Al4V and CoCrMo fabricated by selective laser melting (SLM). Since this initial work, extensive research has been conducted on the topological optimisation of implant geometries to mimic the properties of bone tissue [32]. Shidid et al. [28] present a computationally autonomous just-in-time (JIT) method to algorithmically generate an implant topology for SLM-fabricated lattice structures that is conformal to the surgical resection with mechanical properties that are statistically indistinguishable from the parent bone.

✉ M. Leary
martin.leary@rmit.edu.au

¹ RMIT Centre for Additive Manufacture, School of Engineering, RMIT University, Melbourne, VIC 3000, Australia

² ARC Training Centre in Additive Biomanufacturing, Brisbane QLD 4059, Australia

³ Siemens AG, Power and Gas, Huttenstr. 12, 10553 Berlin, Germany

⁴ Department of Surgery, St. Vincent's Hospital, Melbourne VIC 3000, Australia

Despite the associated commercial opportunities, the geometric definition of MAM lattice structures is potentially complex. For example, McMillan et al. [24, 25] report that data management and computational processing costs are potentially very high, thereby restricting the commercial application of AM technologies.

This research proposes a novel strategy for the digital representation of lattice geometries, whereby strut elements are represented by a polygonal prism. This representation is fundamentally efficient in comparison with equivalent stereolithographic (STL) data generated directly from CAD tools. Furthermore, the method allows direct control of the associated polygon order for each strut element. This research hypothesises that polygon order can be intentionally set at a lower level than may otherwise be used, according to the scenario, without compromising lattice manufacturing dimensional precision.

To assess this hypothesis, lattice strut elements are fabricated with permutations of relevant design parameters, including strut diameter, angle of inclination to the powder bed, polygon order and material type. For these specimens, the circularity of manufactured specimens is assessed according to their isoperimetric quotient and effective diameter. Regression analysis identifies the causality of the design variables on the dependant variables of interest.

This initial research characterises the effects of lattice design and polygon order on the geometric quality of manufactured strut elements. This outcome potentially allows AM data file size reduction without compromising build quality, thereby enabling decreased AM lattice processing time and computational costs.

2 Additive manufacture

AM refers to fabrication by the sequential addition of unit materials [35] based on some digital representation of the intended specimen geometry and supporting structure [34]. According to ISO/ASTM [13], AM is a process of “additive shaping” which is fundamentally different from “subtractive shaping” methods (milling, turning, drilling etc.), as it relies on the addition of material as opposed to the subtraction of material from a workpiece. This novelty provides commercial and technical opportunities, including the fabrication of highly complex structures that are technically infeasible with traditional methods [3]; mass-customised design and product design [31]; reduced environmental impact of manufacture [7]; and increased design complexity [10].

2.1 Metal additive manufacture

Metal additive manufacturing (MAM) is a category of AM that uses metallic input materials [2]. Powder bed

fusion (PBF) is a classification of MAM processes whereby a discrete powder layer is deposited on a bed and then selectively fused by a travelling heat source [5], typically a laser or electron beam, and shielded from oxidation by a vacuum or inert gas [19]. The powder bed then descends by a finite distance, such that geometry is iteratively generated [11].

Commercial PBF systems are technically refined and can achieve high geometric resolution, with useful production rates, part density approaching 100% and robust mechanical properties [8]. Process optimisation studies enable clear understanding of robust operating input parameters, for example as reported by Promopatum et al. [26] for direct metal laser sintering (DMLS) process applied to titanium (Ti-6Al-4V). The technical maturity of PBF systems enables significant innovation in engineering design. For example, the design and fabrication of dental and implant structures with patient-specific geometry [9]; complex lattice structures with exceptional engineering properties [20]; implant structures that are functionalised with bioactive compounds [30] and conformal cooling structures within H13 tool steel mold inserts [20] that demonstrate an improvement in thermal efficiency [23].

2.2 PBF manufacturing defects

Despite its inherent economic and technical advantages, PBF is associated with several specific defect types. Specific defects of relevance to this research are (Fig. 1) stairstepping, slumping, partially adhered particles and solidification errors [9].

Stairstepping is inherent to the PBF process and occurs due to the discretisation of continuous input data to a series of sequential layers [16]. Stairstepping only occurs in geometries which are inclined relative to the powder bed. It is exacerbated for large layer thickness and when geometry is acute to the build platform [18]. Methods for characterising the effects of stairstepping for AM systems are presented by Ahn et al. [1] and applied for SLM by Strano et al. [29].

The PBF process locally fuses geometry with a high-intensity heat source such as a laser or electron beam. This heat source generates a local melt pool by the interaction of multiple, transient physical phenomena [25]. Melt pool dynamics and solidification is challenging to predict numerically [8]; however, experimental observation indicates a number of PBF defects in relation to melt-pool solidification, including slumping, bulk distortion, balling and partially attached powder particles [26].

The solidifying melt pool is supported by previously fused material and the underlying powder bed. Heat transfer from the melt pool to the powder bed causes local heating. When heating is sufficient to locally melt powder, the bulk melt pool

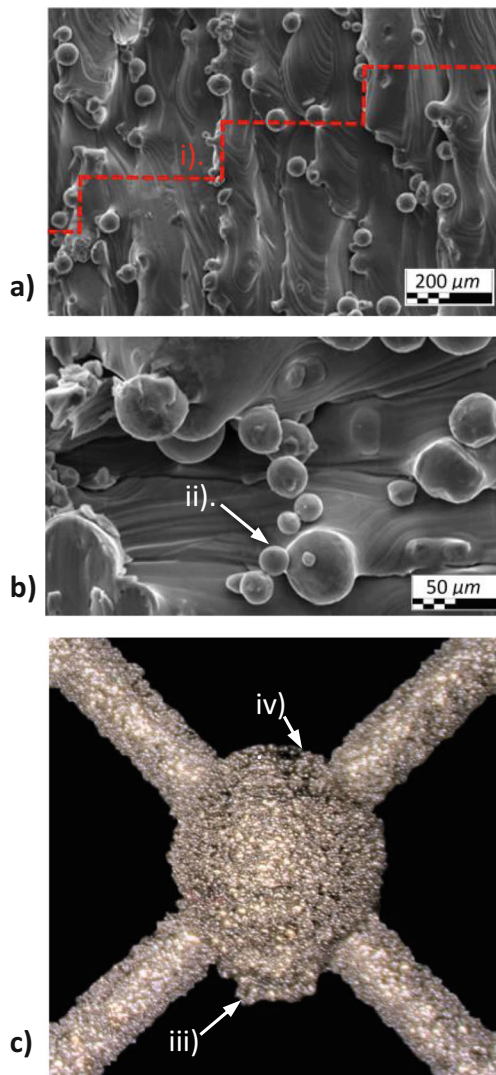


Fig. 1 Manufacturing defects associated with PBF processes. (a) The stairstepping effect (i). (b) Partially melted particles (ii). (c) Slumping (iii) and distortion of molten zone (iv)

distorts towards the powder bed; this phenomenon is known as slumping. When heating is sufficient to partially melt powder particles, these particles become fused to the bulk geometry, but are physically and microstructurally distinct. On upward facing surfaces, partially melted particles typically occur on the layer boundary, whereas on lower faces, these occur at all locations. Thermal diffusivity (h) is a measure for how readily thermal energy will propagate through a medium (Eq. 1). For materials with large thermal diffusivity, the melt pool tends to expand spherically, reducing the ability for the PBF process to correctly represent the intended geometry.

$$h = \frac{k}{\rho C_p} \quad (1)$$

where k is thermal conductivity, ρ is density and C_p is specific heat.

2.3 Powder materials

Metal powder is produced by a range of methods, resulting in powder with a stochastic distribution of spheroidicity and mean diameter. This distribution is often reported by the experimentally derived distribution of mean diameter and by the diameter that represents the 10th (Dv10), 50th (Dv50) and 90th percentiles (Dv90), as well as the surface area moment mean D[3,2] and volume/mass moment mean D[4,3]. The particle size distributions for the materials used in this research are presented in Fig 2.

Relevant data for the materials used in this research are presented in Table 1, including thermal conductivity, density, specific heat and the associated thermal diffusivity.

3 AM data management

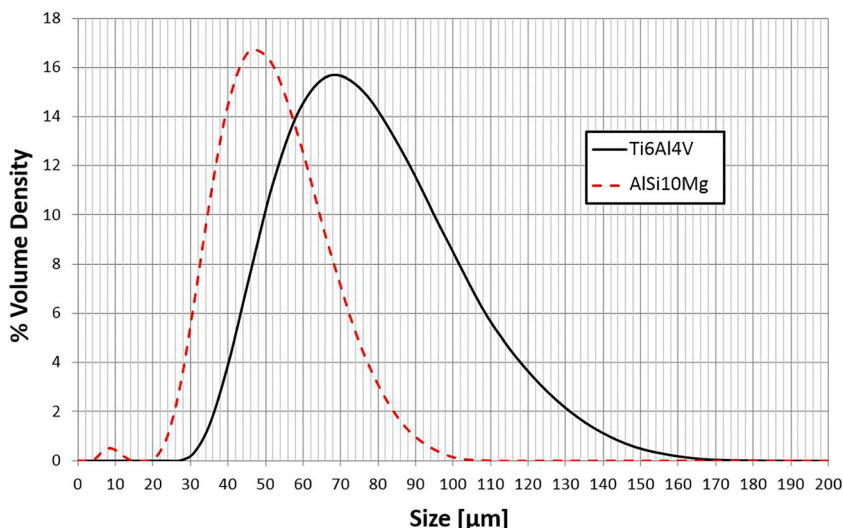
Additive manufacture is fundamentally based on a digital representation of the intended geometry [10]. This digital input is typically based on the STL format which represents volumetric geometry with a finite number of triangular facets [17]. The discrete representation of the STL format potentially introduces geometric error and provides poor storage efficiency [12]. This efficiency is especially poor for AM lattice structures due to the large number of strut sections with high aspect ratio [33].

Due to the inefficiency of the STL format, alternate digital representations are being developed. These alternates include the ISO developed, open-source additive manufacturing format (AMF) [14]. Whether the AM digital input data is based on traditional STL or enhanced methods, this research provides a method for enabling the input data to be matched to manufactured geometry.

Table 1 Powder morphology, thermal properties and MAM process parameters for materials considered in this work. Thermal properties are representative values reported for solid material at room temperature

Material		Ti6Al4V	AlSi10Mg
Powder size distribution	Dv10 (μm)	48.9	32.7
	Dv50 (μm)	73.3	49.5
	Dv90 (μm)	110	71.9
	D[3,2] (μm)	70.0	42.2
	D[4,3] (μm)	76.9	50.6
Histogram of volume density		Fig. 2	
Thermal conductivity, k (W/K)		7.2	140
Density, ρ (kg/m ³)		4471	2680
Specific heat, C_p (J/kgK)		562	900
Thermal diffusivity, h ($\times 10^{-6}$ m ² /s)		2.9	58
Layer thickness (μm)		30	50
Focal offset (μm)		0	2
Laser power (W)		175	350
Energy density (J/mm ³)		68.5	40

Fig. 2 Histogram of volume density versus particle size for Ti6Al4V and AlSi10Mg



4 Design of experiments

This research hypothesises that the circularity of PBF manufactured lattice struts is dependent on material, cross-sectional geometry, diameter and inclination of the strut centreline to the powder bed. The following experimental design of experiments (DOE) is established to assess this hypothesis. This section is split into 3 subsections; the first subsection covers the chosen method for measuring circularity, the isoperimetric quotient and applied statistical methods. The second subsection details the cross-sectional geometries used to compare circularity. The third subsection details part design for analysis of cross sections and their subsequent computed microtomography (μ CT).

4.1 Isoperimetric quotient and statistical analysis

Circularity can be defined by various metrics depending on the specific engineering requirements. For form and fit applications, circularity may be defined by the difference between the diameter of inscribed and circumscribing circles [15]. Alternately, circularity may be defined as the isoperimetric quotient (Q), the ratio of the area of a closed curve (A_c) to the area of a circle (A_p) with equal perimeter (p) to the closed curve (Eq. 4) [6]. Where the radius of a circle with a perimeter equal to the closed curve's (r_p) is:

$$r_p = \frac{p}{2\pi} \tag{2}$$

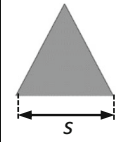
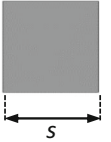
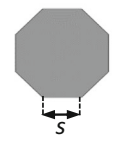
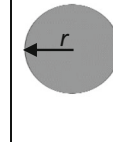
				
	a.	b.	c.	d.
P	3	4	8	∞
$s(A_c)$	$2 \frac{\sqrt{A_c}}{\sqrt{3}}$	$\sqrt{A_c}$	$\left(\frac{A_c}{2(1+\sqrt{2})}\right)^{\frac{1}{2}}$	\sim
$A_c(s)$	$\frac{\sqrt{3}}{4}s^2$	s^2	$(2+2\sqrt{2})s^2$	\sim
D_{eff}	$\frac{\sqrt{3}}{\pi}s$	$\frac{2}{\sqrt{\pi}}s$	$\left(\frac{8}{\pi}(1+\sqrt{2})s^2\right)^{\frac{1}{2}}$	$2r$

Fig. 3 Polygons and associated polygon order (P) used in this research, including relationships for side length (s) cross-sectional area (A_c) and effective diameter of equal circular area (D_{eff}) a. triangle, b. square, c. octagon, d. circle

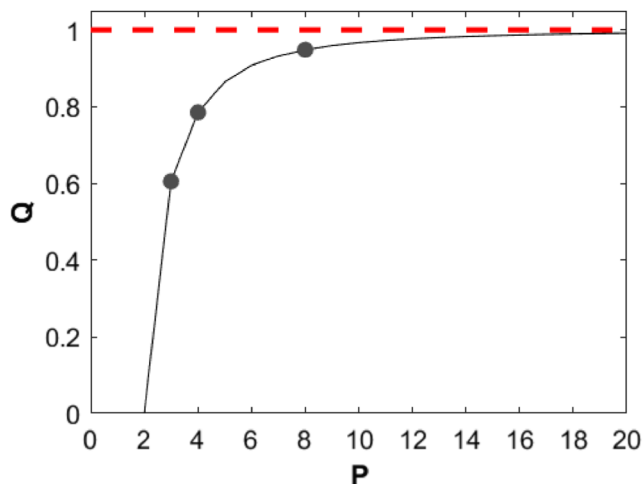


Fig. 4 Isoperimetric quotient (Q) of polygons of order P . Dashed line indicates Q for $P \rightarrow \infty$. Polygons applied in this work are identified (Fig. 3)

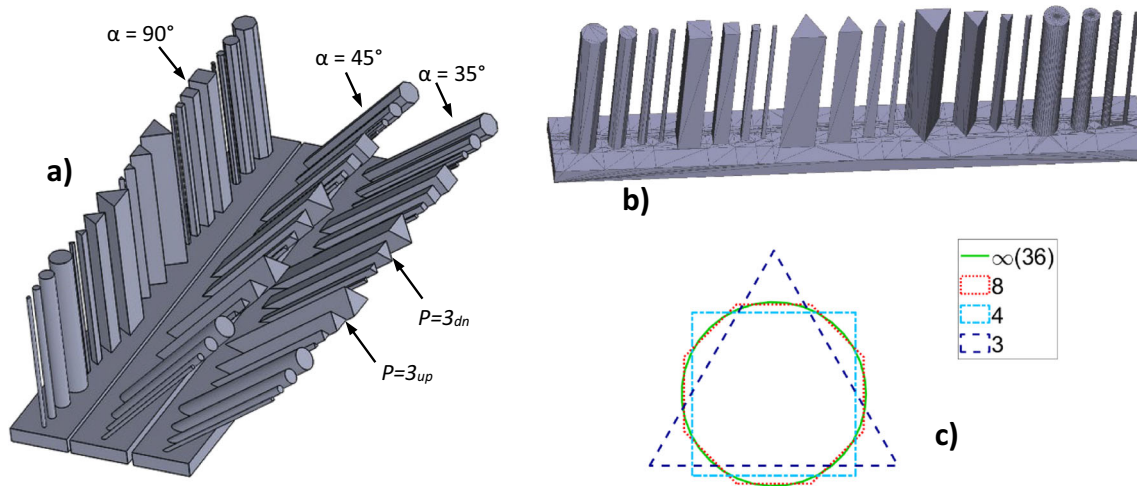


Fig. 5 (a) Experimental array of lattice strut elements according to specified independent (Table 2). (b) Tessellated experimental array of lattice strut elements. (c) Schematic of circular cross section versus other polygon order sections

And the radius of a circle with an equivalent area to the curve (r_c) is:

$$r_c = \sqrt{\frac{A_c}{\pi}} \tag{3}$$

The isoperimetric quotient can then be written in terms of the closed curve’s area (A_c) to its perimeter (p) as:

$$Q = \frac{A_c}{A_p} = \frac{r_c^2}{r_p^2} = \frac{\left(\frac{A_c}{\pi}\right)}{\left(\frac{p}{2\pi}\right)^2} = \frac{4\pi A_c}{p^2} \tag{4}$$

The effective diameter (D_{eff}) is defined as the diameter of a circle that has equal area to that of the closed curve in question and is given as

$$D_{eff} = 2\sqrt{\frac{A_c}{\pi}} \tag{5}$$

4.2 Polygon order

The polygon order (P) describes the number of equally spaced linear segments, used to generate the cross-sectional geometry

Table 2 Design parameters. Polygon order $P = 3$ is assessed in downward and upward configurations

Material	Angle (α)	Nominal diameter (D_{nom}) [mm]	Polynomial order (P)
AlSi10Mg	35°	2.0	∞
Ti6Al4V	45°	1.0	8
		0.5	4
	90°	0.2	3 _{up}

to be manufactured. Three polygon orders were analysed ($P = 3, 4, 8$) to compare with the reference circular geometry ($P \rightarrow \infty$), and are displayed in Fig. 3. Manipulation of the polygon arc length (s) allows the area of the polygon to be maintained to that of a reference circle with a specified nominal diameter (D_{nom}). As P increases, the isoperimetric quotient tends towards that of a perfect circle (i.e. as $P \rightarrow \infty$, $Q \rightarrow 1.0$) as shown in Fig. 4.

4.3 Lattice strut experimental array and data obtainment

A physical lattice element structure was designed (Fig. 5) to enable a relevant experimental DOE to be established for independent variables: nominal strut diameter (D_{nom}); strut centreline inclination angle (α) and polygon order (P) (Table 2). For this initial study, inclination angles useful for the design of lattice structures were selected, specifically, $\alpha = 90^\circ, 45^\circ$, and 35° are specified for vertical support, face centred and body centred structures, respectively [21, 22]. Lattice strut elements were oriented such that a symmetry plane, defined by the strut axis and side face normal, was oriented to align with the powder bed. For the case of triangular cross section ($P = 3$), the two orientations which meet this requirement, identified as *downward* ($P = 3_{dn}$) and *upward* ($P = 3_{up}$), were included (Fig. 5).

A total of 120 permutations of DOE variables were fabricated with SLM using the process parameters of Table 1. Computed microtomography (μ CT) was used to acquire geometrical data of as-manufactured specimens. The μ CT was performed to a voxel size of $8 \mu\text{m}$, enabling qualitative and quantitative inspection of the effect of DOE variables on lattice strut geometry. Custom scripts were developed to process μ CT data into individual slices, perpendicular to the strut inclination axis, and to extract the associated isoperimetric

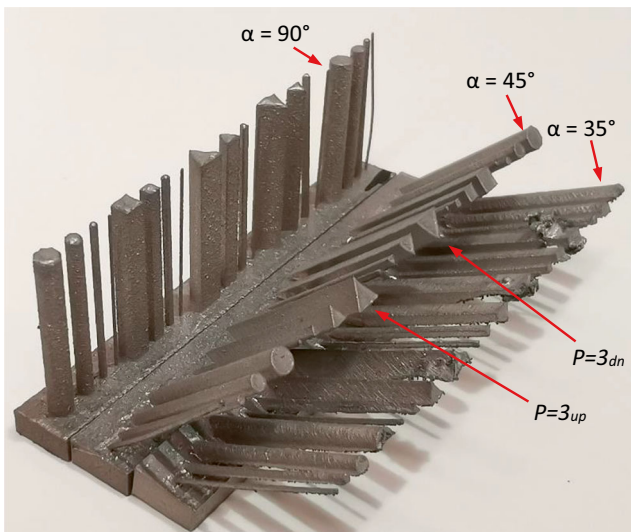


Fig. 6 Fabricated lattice strut experimental array showing various build inclination angles (α) as well as the upwards and downwards facing triangular cross sections ($P = 3_{dn}$ and $P = 3_{up}$, respectively)

quotient and effective diameter. In this research, the effective diameter and the isoperimetric quotient provide useful single-value objective functions. Multiple regression analysis was conducted to study the contribution of geometric parameters: polygon order (P), inclination (α) and nominal diameter (D_{nom}) on dependant variables of interest: isoperimetric quotient (Q) and effective diameter (D_{eff}).

5 Results

Qualitative and quantitative observations for the manufactured specimens are summarised in the following sections. The results section is split into 5 subsections with the first an overview of the μ CT scan reconstructions. The second

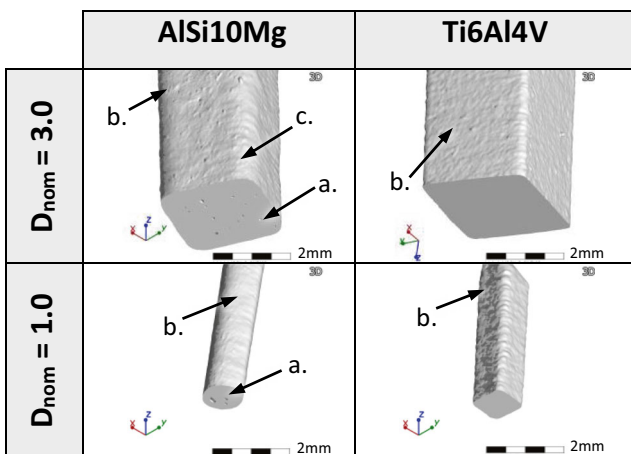


Fig. 7 μ CT image of aluminium and titanium strut specimens for polygon order, $P = 4$ and nominal diameter (D_{nom}) 1 mm and 3 mm. (a) Pore defects. (b) Adhered particles. (c) Rounding of intended geometry. For a given nominal diameter, AlSi10Mg has higher circularity than Ti6Al4V

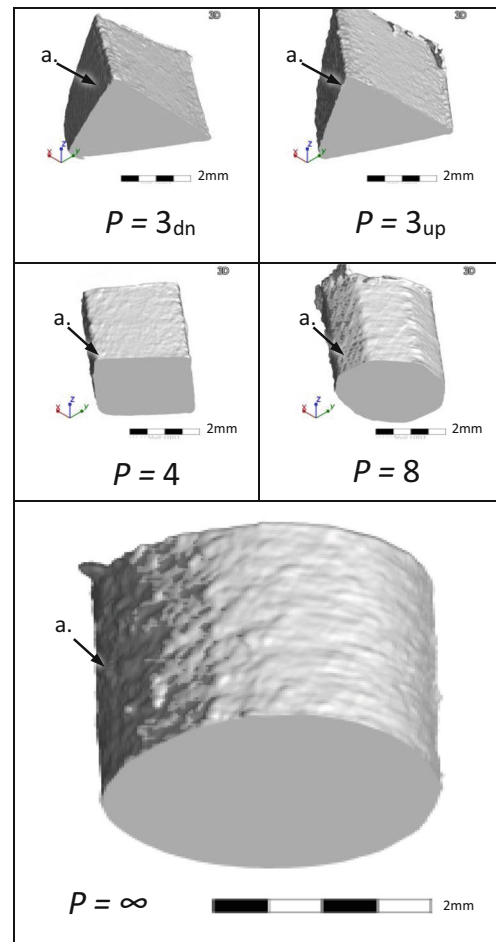


Fig. 8 μ CT of Ti6Al4V strut specimens manufactured at an orientation of $\alpha = 35^\circ$, and nominal diameter, $D_{nom} = 3$ for various polygon order (P). All specimens show increased roughness on faces with downward facing surfaces (a)

and third subsections display the qualitative and quantitative analysis of strut circularity, respectively. The final two subsections display results from the multiple regression analysis with each subsections focusing on the different materials. Fig. 6 displays a fabricated lattice strut experimental array.

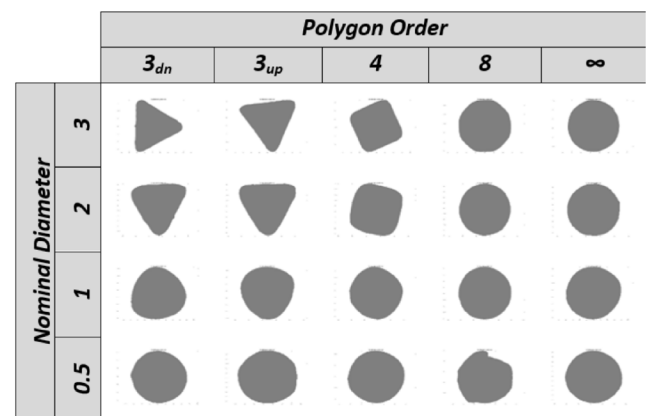


Fig. 9 AlSi10Mg cross sections for $\alpha = 90^\circ$

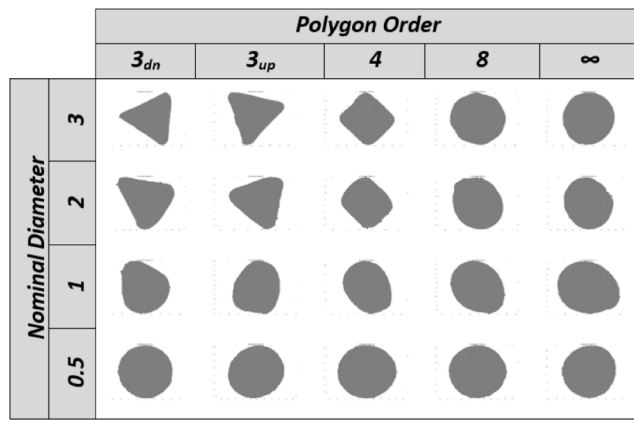


Fig. 10 AlSi10Mg cross sections for $\alpha = 45^\circ$

5.1 μ CT scan results

Both aluminium and titanium materials show adhered particles and rounding of the intended geometry, especially with reducing diameter (Fig. 7). However, it is apparent that aluminium displays a significantly greater tendency to introduce error in following square edges.

For all materials, diameter and polygon order, the effect of inclination angle is to increase roughness on downward facing surfaces. The effect is more pronounced for more acute inclination and for larger diameter specimens (Fig. 8).

5.2 Qualitative observations of circularity

The developed custom script was used to extract cross-sectional images from μ CT data (Figs. 9, 10, 11, 12, 13 and 14). In general, the cross-sectional images display a visual increase in circularity for increasing polygon order, in both aluminium and titanium struts. However, below nominal diameters of 1 mm ($D_{nom} \leq 1$ mm), this statement does not hold true for aluminium, with cross sections becoming largely circular in shape for all polygon orders. For titanium struts, the level of circularity for polygon orders: 3, 4 and 8 is lower than that of aluminium sections with equal polygon order and

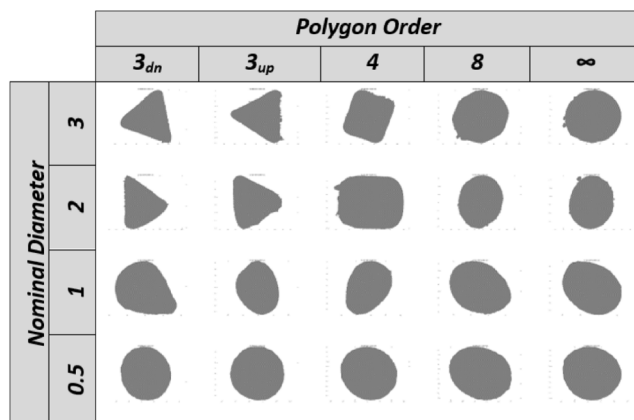


Fig. 11 AlSi10Mg cross sections for $\alpha = 35^\circ$

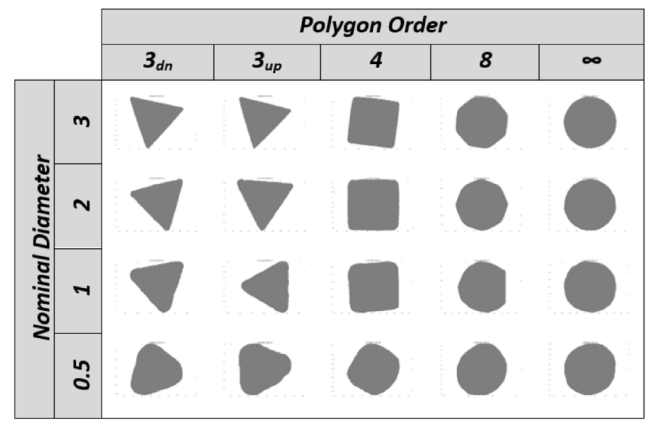


Fig. 12 Ti6Al4V cross sections for $\alpha = 90^\circ$

nominal diameter. In general, although circularity of these specimens increases with decreasing nominal diameter, Ti6Al4V cross sections retain evidence of their polygon order for $P \leq 4$. For both materials, the specimen-cross section skews in the direction of the powder bed with increasing inclination angle.

5.3 Quantitative observations of circularity

The isoperimetric quotient (Q) and effective diameter (D_{eff}) were extracted from the cross-sectional images using the custom developed script. Figures 15, 16, 17, 18, 19 and 20 graphically summarise pertinent attributes of this data. Fig. 15 displays a varying isoperimetric quotient (Q) for different nominal diameters (D_{nom}). In general, higher polygon order geometries display higher Q , indicating a more circular cross section. As D_{nom} decreases, Q tends to increase, i.e. for $D_{nom} = 3.0$, $\min(Q) \approx 0.3$, but for $D_{nom} = 0.5$, $\min(Q) \approx 0.6$. The variation in Q within groups of P appears to increase with an increasing D_{nom} . A variation in effective diameter (D_{eff}) is observed for these manufactured specimens (Fig. 16).

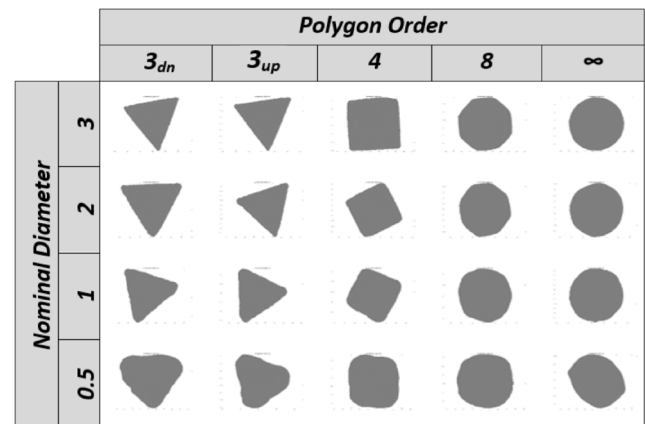


Fig. 13 Ti6Al4V cross sections for $\alpha = 45^\circ$

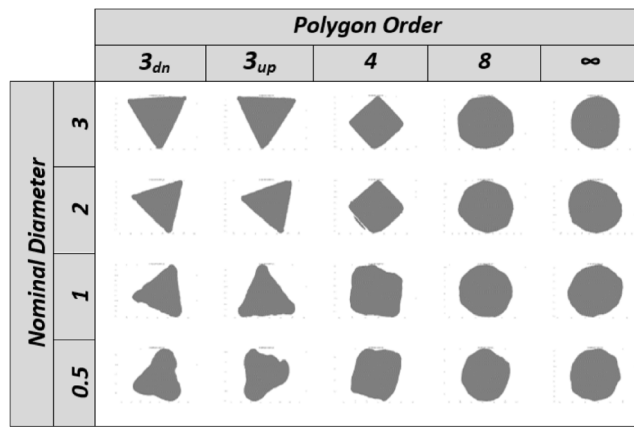


Fig. 14 Ti6Al4V cross sections for $\alpha = 35^\circ$

The diameter ratio (\bar{D}_{eff}/D_{nom}), where \bar{D}_{eff} is the mean D_{eff} , provides greater insight into the effect of material and D_{nom} on the strut effective diameter (D_{eff}) (Figs. 17 and 18). As D_{nom} tends to zero, D_{eff} generally increases according to the limiting minimum feature size achievable with the specific process parameters and materials. From the evaluated DOE, it is apparent that there are conditions in which a \bar{D}_{eff}/D_{nom} will result in a value of 1 (effective diameter equals nominal diameter). This outcome suggests that smart geometric design can lead to a fabricated strut cross section equal to that of the intended cross section for any value of D_{nom} .

The effect of triangle orientation, nominal diameter and material upon effective diameter (D_{eff}) is assessed in Figs. 19 and 20. It is apparent that \bar{D}_{eff}/D_{nom} tends to increase for reducing value of D_{nom} , except for vertical triangular AlSi10Mg struts with nominal diameter of 0.5 mm. These triangular struts exhibit a \bar{D}_{eff}/D_{nom} ratio less than 0.7, suggesting these struts are undersized. A broadened DOE is required to ascertain whether any significant effects can be assigned to triangle orientation.

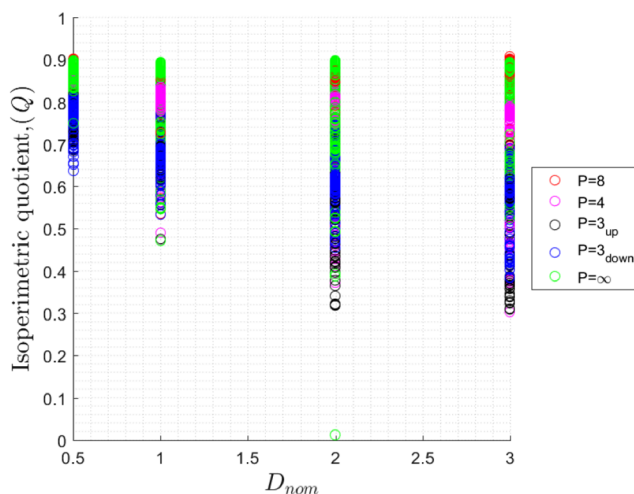


Fig. 15 Isoperimetric quotient (Q) versus nominal diameter (D_{nom})

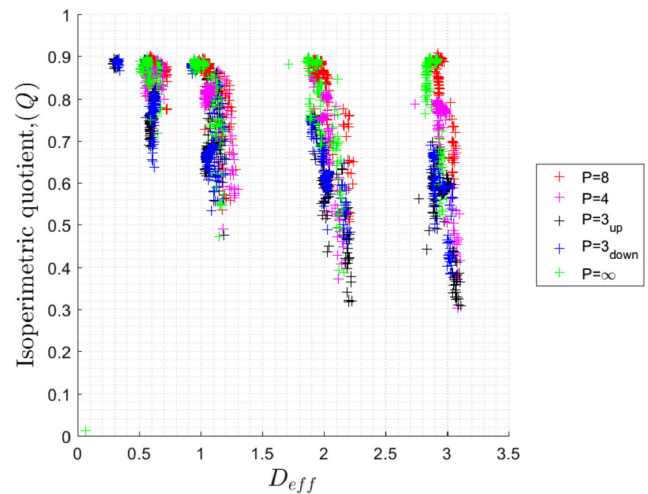


Fig. 16 Isoperimetric quotient (Q) versus effective diameter (D_{eff})

5.4 Regression analysis—titanium Ti6Al4V

Observations from multiple regression analysis found that in general as strut diameter decreases, the circularity of all investigated polygons increases. This relationship confirms the existence of a threshold, below which a low polygon order geometry can represent lattice strut geometries without error. For fabricated triangular cross sections ($P = 3$), the polygon orientation influences associated roughness and circularity, with downward facing triangles ($P = 3_{dn}$), having lower roughness. The fabricated struts material type also influenced circularity and error in target diameter (D_{nom}), with aluminium having greater associated error than titanium.

For Ti6Al4V, the relationship between the isoperimetric quotient and independent geometric variables is assessed by the stepwise regression method. By including independent variables, plus products of these variables and squared terms, it results in a predictive equation for isoperimetric quotient ($Q_{Ti6Al4V}$), with correlation coefficient ($R^2 = 0.847$) (Eq. 6).

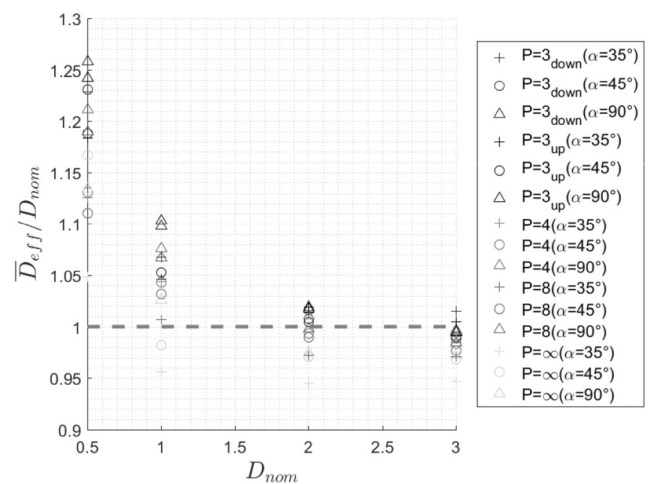


Fig. 17 Diameter ratio, \bar{D}_{eff}/D_{nom} for Ti6Al4V. Dashed line indicates $\bar{D}_{eff}/D_{nom} = 1.0$. Marker colour indicates P , shape indicates α

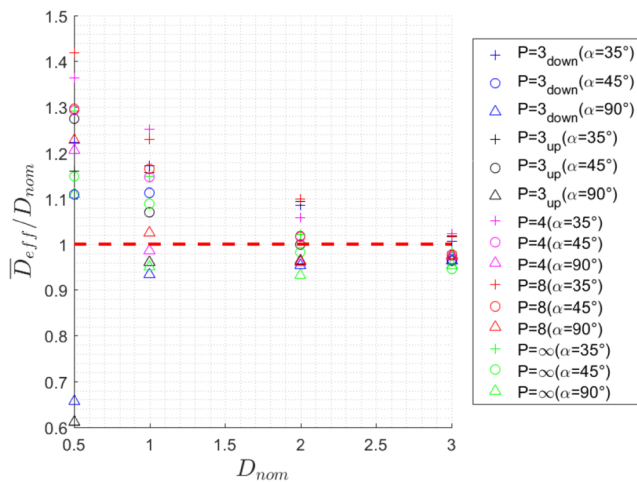


Fig. 18 Diameter ratio, \bar{D}_{eff}/D_{nom} for AlSi10Mg. Dashed line indicates $\bar{D}_{eff}/D_{nom} = 1.0$. Marker colour indicates P , shape indicates α

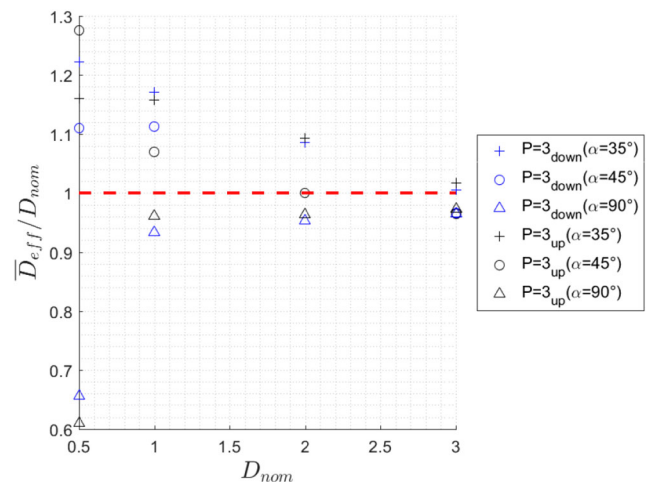


Fig. 20 AlSi10Mg triangle. Dashed line indicates $\bar{D}_{eff}/D_{nom} = 1.0$

For this predictive equation, the contributions of independent variables to R^2 are polygon order, 76%; nominal diameter, 17%; and inclination angle, 4%. This insight enables the reduced order predictive equation with fewer variables, while achieving $R^2 = 0.695$ (Eq. 7).

$$Q_{Ti6Al4V} = 0.3645 + 0.10824P + 0.006319\alpha - 0.15858D_{nom} - 0.007544P^2 - 0.000040\alpha^2 + 0.02281D_{nom}^2 - 0.000068P\alpha + 0.011209PD_{nom} - 0.000201\alpha D_{nom}, R^2 = 0.847 \quad (6)$$

$$Q_{Ti6Al4V} = 0.03292P - 0.02732D + 0.64035, R^2 = 0.695 \quad (7)$$

Similarly, a predictive equation can be developed for effective diameter ($D_{eff, Ti6Al4V}$), with correlation coefficient

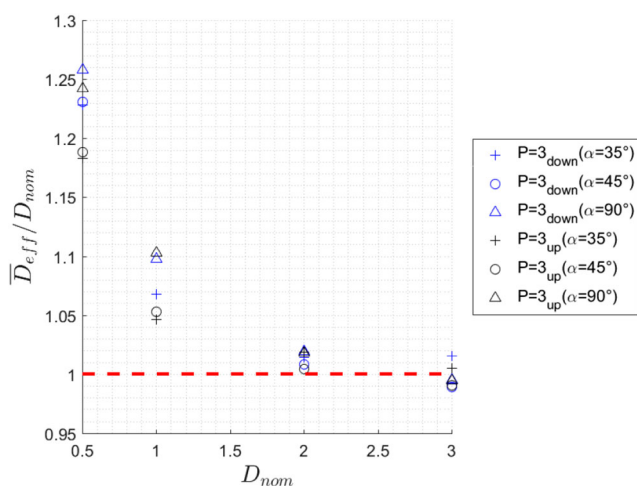


Fig. 19 Ti6Al4V triangle. Dashed line indicates $\bar{D}_{eff}/D_{nom} = 1.0$

($R^2 = 0.999$) (Eq. 8). In this scenario, the contributions of independent variables to R^2 are P , 0.098%; D_{nom} , 99.85%; and α , 0.029%; this allows a reduced order predictive equation with $R^2 = 0.998$ (Eq. 9).

$$D_{eff, Ti6Al4V} = 0.12195 - 0.00128P + 0.92240D_{nom} - 0.000802\alpha - 0.000802P^2 + 0.011537D_{nom}^2 - 0.002100PD_{nom} + 0.000056P\alpha - 0.000078D_{nom}\alpha, R^2 = 0.999 \quad (8)$$

$$D_{eff, Ti6Al4V} = 0.1079 + 0.9450D_{nom}, R^2 = 0.9983 \quad (9)$$

5.5 Regression analysis—aluminium AlSi10Mg

By similar methods as those applied to titanium struts, regression relationships are identified for $Q_{AlSi10Mg}$ (Eq. 10), with $R^2 = 0.728$, and contributions to R^2 : D_{nom} , 46% and α , 27.5%; P , 16.5%, allowing a reduced order predictor with $R^2 = 0.554$ (Eq. 11).

$$Q_{AlSi10Mg} = 0.4876 + 0.01247P + 0.01739\alpha - 0.3954D_{nom} - 0.001700P^2 - 0.000128\alpha^2 + 0.04386D_{nom}^2 - 0.000066P\alpha + 0.016759PD_{nom} + 0.001267\alpha D_{nom}, R^2 = 0.728. \quad (10)$$

$$Q_{AlSi10Mg} = 0.6433 + 0.016741P - 0.08487D_{nom} + 0.002817\alpha, R^2 = 0.554 \quad (11)$$

Regression for $D_{eff, AlSi10Mg}$ (Eq. 12) provides $R^2 = 0.994$, with contributions to R^2 : D_{nom} , 99.05% and α , 0.71%; P ,

0.12%, allowing a reduced order predictor or $D_{\text{eff,AISi10Mg}}$ with $R^2 = 0.984$ (Eq. 13).

$$D_{\text{eff,AISi10Mg}} = 0.5135 + 0.09911P + 1.0242D_{\text{nom}} - 0.02141\alpha - 0.008193P^2 - 0.02312D_{\text{nom}}^2 + 0.0001\alpha^2 - 0.006866PD_{\text{nom}} + 0.00014P + 0.000614D_{\text{nom}}\alpha, R^2 = 0.994 \quad (12)$$

$$D_{\text{eff,AISi10Mg}} = 0.1344 + 0.9382D_{\text{nom}}, R^2 = 0.984 \quad (13)$$

Regression analysis of the experimental DOE provides insight into the causality of geometric lattice parameters for materials of interest. Particularly, that robust correlation can be obtained for titanium Ti6Al4V ($R^2 = 0.847$) and aluminium AISi10Mg ($R^2 = 0.728$) with the independent variables selected for this work. The causality of independent variables are dependent on material selection; for titanium, polygon order (P) is dominant for predicting the isoperimetric quotient, for aluminium, nominal diameter (D_{nom}) is dominant.

6 Concluding remarks

Additive manufacture enables the fabrication of innovative lattice structures; however, the commercialisation of these structures is potentially limited by the efficiency of characterising AM lattice geometry. This research responds to the hypothesis that the circularity of AM lattice structures is a function of geometric lattice parameters and material of manufacture.

To provide initial insight, a preliminary DOE was devised and fabricated using SLM for titanium Ti6Al4V and aluminium AISi10Mg. Custom scripts were developed to assess μCT data to allow qualitative and quantitative analysis of lattice strut circularity. This research provides the following fundamental insights into the effect of polygon order on AM manufacturability:

- Qualitative observation of μCT cross-sectional images suggests that the combination of a low polygon order ($P \leq 4$) and nominal diameter (D_{nom}) can be used as circular cross-section surrogates. This observed effect is stronger in aluminium AISi10Mg, than for titanium (Ti6Al4). Also a reduction in build inclination angle (α) tends to result in elongation of a struts cross section.

- The stepwise regression method applied to obtain robust predictive relationships for Q_{Ti6Al4V} ($R^2 = 0.847$), Q_{AISi10Mg} ($R^2 = 0.728$), $D_{\text{eff,Ti6Al4V}}$ ($R^2 = 0.999$) and $D_{\text{eff,AISi10Mg}}$ ($R^2 = 0.994$).
- Reduced order predictive models are also proposed based on the most causal predictive variables. For Ti6Al4V, the struts polygon order has the greatest significance on Q , followed by D_{nom} . While for D_{eff} , the only significant variable is D_{nom} . For AISi10Mg, all three variables influence Q , with D_{nom} being the most significant. Meanwhile, D_{nom} is the only significant influence on D_{eff} . In terms of the isoperimetric quotient (Q), these findings suggest a fundamental difference between the response of titanium and aluminium during AM.
- Outcomes from this research confirm that geometric thresholds exist, below which additional geometric resolution does not result in increased part quality. These thresholds are predominantly caused by polygon order (P) and nominal diameter (D_{nom}). The effect of inclination angle (α) is less significant. It is a noteworthy observation that the causality observed between inclination angle (α) and isoperimetric quotient is low; however, there is an observed effect on effective diameter (D_{eff}).
- The inclination angle (α) was qualitatively observed to increase cross-section skewness towards the powder bed. This outcome suggests alternate input geometries are required to achieve consistently circular cross sections, by offsetting the elongating effect of inclination angle.
- The orientation of a fabricated triangular struts cross section ($P = 3$) appears to influence local roughness at build inclination angles below 90° . Downward facing triangular cross sections $P = 3_{\text{dn}}$ give the impression of lower surface roughness when compared with upward facing triangular cross sections $P = 3_{\text{up}}$. Further research is required to quantify this effect.
- The proposed technique of matching nominal diameter (D_{nom}) to the equivalent polygon side length (s) (Fig. 3) provides a robust method to obtain a specific effective diameter (D_{eff}) as observed by the very high correlation coefficients of Eqs. 9 and 13.

These findings confirm that reduction in the computational cost associated with representing AM lattice geometries is achievable without compromising engineering outcomes. These preliminary outcomes provide guidance for future work to further quantify the effects of geometric and material parameters on the geometric qualities of MAM lattice structures, and allow the direct integration of cost-optimal geometric conditions within algorithmic methods for the AM lattice design.

Acknowledgements The authors acknowledge use of facilities within the RMIT Advanced Manufacturing Precinct and the RMIT Microscopy and Microanalysis Facility. This research was conducted by the Australian Research Council Industrial Transformation Training Centre in Additive Bio manufacturing (IC160100026) <http://www.additivebiomanufacturing.org>.

References

- Ahn D, Kim H, Lee S (2009) Surface roughness prediction using measured data and interpolation in layered manufacturing. *J Mater Process Technol* 209(2):664–671
- ASTM standard F2792-12a, D (2012) F2792-12a. Standard terminology for additive manufacturing technologies. ASTM International, West Conshohocken
- Berman B (2012) 3-D printing: the new industrial revolution. *Bus Horiz* 55(2):155–162
- Brandt M, Sun SJ, Leary M, Feih S, Elambasseril J, Liu QC (2013) High-value SLM aerospace components: from design to manufacture. *Adv Mater Res* 633:135–147
- Clijsters S, Craeghs T, Buls S, Kempen K, Kruth JP (2014) In situ quality control of the selective laser melting process using a high-speed, real-time melt pool monitoring system. *Int J Adv Manuf Technol* 75(5-8):1089–1101
- Croft HT (1991) Unsolved problems in geometry: unsolved problems in intuitive mathematics. Springer New York, New York
- Drizo A, Pegna J (2006) Environmental impacts of rapid prototyping: an overview of research to date. *Rapid Prototyp J* 12(2):64–71
- Frazier WE (2014) Metal additive manufacturing: a review. *J Mater Eng Perform* 23(6):1917–1928
- Gebhardt A, Schmidt F-M, Hötter J-S, Sokalla W, Sokalla P (2010) Additive manufacturing by selective laser melting the realizer desktop machine and its application for the dental industry. *Phys Procedia* 5:543–549
- Gibson R, Stucker (2010) Additive manufacturing technologies - rapid prototyping to direct digital manufacturing
- Gibson I, Rosen D, Stucker B (2015) Powder Bed Fusion Processes, in *Additive Manufacturing Technologies*. Springer pp 107–145
- Hiller JD, Lipson H (2009) STL 2.0: a proposal for a universal multi-material additive manufacturing file format. In: *Proceedings of the Solid Freeform Fabrication Symposium*
- ISO/ASTM (2015) Additive manufacturing — general principles — terminology. 52900. ISO/ASTM, Geneva 52900
- ISO/ASTM (2016) Standard specification for additive manufacturing file format (AMF) version 1.2
- Jywe W-Y, Liu C-H, Chen C o-K (1999) The min–max problem for evaluating the form error of a circle. *Measurement* 26(4):273–282
- Leary M, Babae M, Brandt M, Subic A (2013) Feasible build orientations for self-supporting fused deposition manufacture: a novel approach to space-filling tessellated geometries. *Adv Mater Res* 633:148–168
- Ma D, Lin F, Chua CK (2001) Rapid prototyping applications in medicine. Part 2: STL file generation and case studies. *Int J Adv Manuf Technol* 18:118–127
- Mani K, Kulkarni P, Dutta D (1999) Region-based adaptive slicing. *Computer-Aided Design* 31: 317–333
- Marcu T, Todea M, Gligor I, Berce P, Popa C (2012) Effect of surface conditioning on the flowability of Ti6Al7Nb powder for selective laser melting applications. *Appl Surf Sci* 258(7):3276–3282
- Mazur M, Leary M, Sun S, Vcelka M, Shidid D, Brandt M (2016) Deformation and failure behaviour of Ti-6Al-4V lattice structures manufactured by selective laser melting (SLM). *Int J Adv Manuf Technol* 84:1391–1411
- Mazur M, Leary M, McMillan M, Elambasseril J, Brandt M (2016a) SLM additive manufacture of H13 tool steel with conformal cooling and structural lattices. *Rapid Prototyp J* 22(3):504–518
- Mazur M, Leary M, McMillan M, Sun S, Shidid D, Brandt M (2016b) Mechanical properties of Ti6Al4V and AlSi12Mg lattice structures manufactured by selective laser melting (SLM). *Laser Additive Manufacturing: Materials, Design, Technologies, and Applications*: 119–161
- Mazur M, Brincat P, Leary M, Brandt M (2017) Numerical and experimental evaluation of a conformally cooled H13 steel injection mould manufactured with selective laser melting. *Int J Adv Manuf Technol*:1–20
- McMillan ML, Jurg M, Leary M, Brandt M (2017a) Programmatic generation of computationally efficient lattice structures for additive manufacture. *Rapid Prototyp J* 23(3):486–494
- McMillan M, Leary M, Brandt M (2017b) Computationally efficient finite difference method for metal additive manufacturing: a reduced-order DFAM tool applied to SLM. *Mater Des* 132:226–243
- Promopattum P, Onler R, Yao S-C (2017) Numerical and experimental investigations of micro and macro characteristics of direct metal laser sintered Ti-6Al-4V products. *J Mater Process Technol* 240:262–273
- Sexton L, Lavin S, Byrne G, Kennedy A (2002) Laser cladding of aerospace materials. *J Mater Process Technol* 122(1):63–68
- Shidid D, Leary M, Choong P, Brandt M (2016) Just-in-time design and additive manufacture of patient-specific medical implants. *Phys Procedia* 83:4–14
- Strano G, Hao L, Everson RM, Evans KE (2013) Surface roughness analysis, modelling and prediction in selective laser melting. *J Mater Process Technol* 213(4):589–597
- Vaithilingam J, Kilsby S, Goodridge RD, Christie SD, Edmondson S, Hague RJ (2015) Functionalisation of Ti6Al4V components fabricated using selective laser melting with a bioactive compound. *Mater Sci Eng C Mater Biol Appl* 46:52–61
- Vandenbroucke B, Kruth JP (2007) Selective laser melting of bio-compatible metals for rapid manufacturing of medical parts. *Rapid Prototyp J* 13(4):196–203
- Wang X, Xu S, Zhou S, Xu W, Leary M, Choong P, Qian M, Brandt M, Xie YM (2016) Topological design and additive manufacturing of porous metals for bone scaffolds and orthopaedic implants: a review. *Biomaterials* 83:127–141
- Williams CB, Cochran JK, Rosen DW (2010) Additive manufacturing of metallic cellular materials via three-dimensional printing. *Int J Adv Manuf Technol* 53(1-4):231–239
- Wong KV, Hernandez A (2012) A review of additive manufacturing. *ISRN Mech Eng* 2012:1–10
- Zhai Y, Lados DA, LaGoy JL (2014) Additive manufacturing: making imagination the major limitation. *Jom* 66(5):808–816

Publisher's note Springer Nature remains neutral with regard to jurisdictional claims in published maps and institutional affiliations.